# Evolutionary variation in MADS-box dimerization affects floral development and protein degradation dynamics

Maria Jazmin Abraham-Juarez[1,2,3], Amanda Schrager-Lavelle[1,2,4], Jarrett Man[2], Clinton Whipple[5], Pubudu Handakumbura[2,6], Courtney Babbitt[2], Madelaine Bartlett*[2]

[1] co-first authors
[2] Biology Department, University of Massachusetts Amherst, USA
[3] IPICYT, San Luis Potosi, Mexico
[4] Biology Department, Colorado Mesa University, USA
[5] Biology Department, Brigham Young University, USA
[6] Pacific Northwest National Laboratory, USA

*Corresponding Author: Madelaine Bartlett

**Email:** mbartlett@umass.edu

**Keywords**
PISTILLATA, evo-devo, flower evolution, transcription factor, floral quartets

**Evolutionary variation in MADS-box dimerization affects floral development and protein degradation dynamics in maize**

Maria Jazmin Abraham Juarez*, Amanda Schrager-Lavelle*, Jarrett Man, Clinton Whipple, Courtney Babbitt, Madelaine Bartlett
*= co-first authors

**Abstract**
The B-class MADS-box transcription factors STERILE TASSEL SILKY EAR1 (STS1) and SILKY1 (SI1) specify floral organ identity in the grass *Zea mays* (maize). STS1 and SI1 bind DNA as obligate heterodimers. Obligate heterodimerization between STS1 and SI1 homologs, although common in flowering plants, arose very recently in the grass family. This recent emergence of obligate heterodimerization from STS1 homodimerization provided an opportunity to test the consequences of evolutionary shifts in MADS-box protein-protein interactions. We tested the ability of evolutionary variation in STS1 dimerization to impact floral development, downstream gene regulation, and protein complex formation in maize. We found that STS1 hetero- vs. homodimerization had subtle effects on protein localization and stamen development. In contrast, differential STS1 dimerization resulted in large-scale changes to gene expression and protein complex composition. We identified kinases and proteins involved in ubiquitylation as candidate interactors with MADS-box proteins, and found that STS1 was phosphorylated, and in a complex with ubiquitylated proteins. In addition, we found that STS1 homodimers were more abundant than STS1-SI1 heterodimers, independent of RNA levels. Thus, differential dimerization can affect both protein degradation dynamics and combinatorial assembly of MADS-box protein complexes. Our results highlight the robustness of floral development to some molecular change, which may contribute to the evolvability of floral form.

**Significance Statement**
Interactions between transcription factors can alter downstream gene expression patterns and, in turn, organismal development. In plants, MADS-box transcription factors specify floral organ identity as part of large complexes. Shifting interactions between MADS-box proteins have been proposed as drivers in the evolution of the flower, and in the diversification of floral form. However, the functional consequences of changes to individual MADS-box protein-protein interactions are unknown. Here, we show that floral development is subtly affected by altered transcription factor protein-protein interactions. We also show that shifting transcription factor interactions can contribute to differential protein degradation. This reveals an important consequence for evolutionary variation in transcription factor interactions, and adds a new layer of complexity to the evolution of developmental gene networks.

**Introduction**
A paradox lies at the heart of floral evo-devo: flower morphology is diverse, but the master regulators specifying floral organ identity are conserved. These master regulators are the floral MADS-box transcription factor genes, first described in *Antirrhinum majus* and *Arabidopsis thaliana.* The original ABC model of floral development was derived from floral mutants, and explains how whorls of floral organs are specified by groups of transcription factors (A- through E-class proteins) (1, 2). In this model, A class genes specify sepal development, A- and B-class genes specify petal development, B- and C-class genes specify stamen development, and C-class genes specify carpel development. The E-class genes specify organ identity in all four whorls, and the D-class genes specify ovule identity. All but one of the original ABCDE genes encode MADS-box transcription factors. These MADS-box proteins are proposed to function as tetramers, or floral quartets, with tetramer composition determining DNA-binding and downstream gene regulation. For example, tetramers of B-, C-, and E-class proteins are proposed to specify stamen identity, and tetramers of C and E-class proteins are proposed to specify carpel identity (3, 4). This model is supported by genetic data, extensive *in vitro* characterization of MADS-box protein-protein interactions, and *in planta* evidence for MADS-box complex formation and DNA-binding by

floral quartets, particularly in *A. thaliana* (reviewed in 4). Outside of the core eudicots, B-class and C-class function, in particular, is deeply conserved (reviewed in 5). For example, B-class genes specify stamen and petal identity in every species for which functional data exists, even when petals are highly modified (6–10). How, then, can floral organs like stamens and petals vary so extensively in form and function, when they are specified by orthologous genes?

The combinatorial assembly of MADS-box protein complexes has been proposed as an answer to this question. Although floral quartets composed of the same protein classes may specify the same floral organs in different lineages, mixing and matching of particular MADS-box proteins in floral quartets may generate floral diversity by regulating different suites of downstream genes. These differences in downstream targets may contribute to evolutionary variation in organ shape and form (11–14). Evolutionary changes to MADS-box complexes may also have been important in the emergence of the flower. A key event in the evolution of the flower was a transition from separate male and female reproductive structures to a single axis bearing both male and female reproductive organs (reviewed in 15). Ancestral sequence analyses indicate that BCE MADS-box complexes, which specify stamen identity, may have evolved along the lineage leading to flowering plants. The emergence of these complexes may have been critical in the emergence of the flower (but see 4, 12, 16). Thus, combinatorial assembly of MADS-box complexes may have been important in floral evolution and diversification.

Although differential MADS-box complex assembly presents an appealing model for explaining floral diversification, the functional consequences of changing MADS-box protein-protein interactions have not been extensively tested *in planta*. The model predicts that (1) MADS-box complexes like the BCE complex should be conserved across flowering plants, and that (2) evolutionary changes to floral MADS-box protein-protein interactions should result in consequent changes to downstream gene regulation, and to floral form. Here, we test these predictions using the B-class MADS box protein STS1 (a homolog of PISTILLATA in *A. thaliana*) (6, 8). In maize, STS1 forms obligate heterodimers with SI1 (a homolog of APETALA3 in *A. thaliana*) (7, 17). We engineered an ancestral variant of STS1 that forms both homodimers and heterodimers with SI1 (18). We show that facultative STS1 homodimerization (vs. obligate heterodimerization between STS1 and SI1) has subtle effects on floral development, but large effects on downstream gene expression and protein-protein interaction networks. We also show that STS1 can be found in complex with C-class and E-class MADS-box proteins. Lastly, we found that STS1 dimerization may affect protein degradation dynamics. Our results show that single changes to MADS-box protein-protein interactions could alter floral development in small ways, but likely act in concert with other changes in the evolution of flower morphology.

## Results

### STS1-HET and STS1-HOM show subtle differences in localization and function

To explore the effects of B-class hetero- vs. homodimerization, we developed transgenic maize plants that express a version of STS1 that can bind DNA as homodimers. In previous work, we found that changing the glycine (G) residue at position 81 to aspartic acid (D) reverts STS1 to its most likely ancestral dimerization state - able to form both homodimers and heterodimers with SI1 (18). Other amino acid residues differ between STS1 and its most likely ancestor. However, we chose to introduce a single change so that we could explicitly test the effects of hetero- vs homodimerization, to the exclusion of other differences between the extant and ancestral proteins. We introduced the critical G81D change into an STS1-yellow fluorescent protein fusion construct (STS1-YFP) that rescues *sts1 (6)*, and used it to transform maize plants. We will refer to the obligate heterodimer construct *(pSTS1::STS1-YFP*) as *STS1-HET*, and to the STS1 homodimer construct (*pSTS1::STS1(G81D)-YFP*) as *STS1-HOM*.

To understand how variable B-class dimerization affects floral development, we used identical crossing schemes to generate lines carrying either *STS1-HET* or *STS1-HOM*, in backgrounds that were segregating either *si1* or *sts1* (6, 7). In both *si1* and *sts1,* stamen and lodicule (petal homolog) organ identity is lost (6,

7). We found that both transgenes complemented *sts1;* neither organ identity nor organ number varied between *STS1-HET* and *STS1-HOM* (Fig. 1, Table S1). In contrast, adult flowers in *si1* mutants carrying *STS1-HOM* were indistinguishable from non-transgenic *si1* mutants (Fig. 1). This indicates that *STS1-HOM* can rescue *sts1* mutants and is functional, but can not compensate for the loss of *SI1* function.

To explore differences between STS1-HET and STS1-HOM in more detail, we analyzed the development of complemented *sts1* mutants. We examined early protein localization of both STS1-HET and STS1-HOM using confocal microscopy. We found that STS1-HET was restricted to lodicule and stamen primordia (Fig. 1 G-H), as expected (6). In contrast, protein localization was relaxed in STS1-HOM lines, appearing in the gynoecia in addition to lodicule and stamen primordia (Fig. 1J). However, this gynoecial localization was not evident in our immunolocalizations using an anti-STS1 antibody (Fig. S1). In contrast to the proteins, *STS1-HET* and *STS1-HOM* RNAs showed similar localization patterns (Fig. S1). This suggests that the subtle localization differences we detected were regulated at the protein level.

In addition to protein localization differences, morphology differed subtly between STS1-HOM and STS1-HET flowers. This included differences in anther aspect ratio, such that anthers of STS1-HOM flowers were wider and shorter than those of STS1-HET flowers while they were still developing (t-test p-value = 6.8e-10, Fig. 1K-L). In contrast, at anthesis, mature anthers of STS1-HOM flowers were longer and thinner than those of STS1-HET flowers (t-test, p-value = 0.003, Fig. 1M-N). These differences were despite similarities in anther surface area, which we used as a proxy for size (developing anthers: t-test p-value = 0.259, Fig 1K; anthesis: t-test p-value = 0.367, Fig. 1M). These results suggest that B-class dimerization may affect anther growth dynamics. Similarly, B-class gene expression affects developmental dynamics in *A. thaliana,* where B-class genes are important for both early and late floral organ development (19). We also assayed mature anther shape using eFourier analysis using the R package MOMOCS (20). This analysis identified a small, but significant difference in shape between anthers from *sts1* mutants complemented with either *STS1-HET* or *STS1-HOM* (Fig. S2). Thus, differential B-class dimerization may have subtle effects on developmental dynamics and anther dimensions.

**Differential dimerization of maize B-class proteins affects downstream gene regulation**

The localization and morphological differences between *STS1-HET* and *STS1-HOM* flowers were subtle, suggesting small phenotypic consequences of differential B-class dimerization. We were curious if molecular function was similarly conserved between *STS1-HET* and *STS1-HOM*. To understand the effect of STS1 dimerization on gene expression, we performed RNA-seq analysis in *sts1* or *si1* mutants complemented with either *STS1-HET* or *STS1-HOM*. We harvested inflorescence tissue shortly after stamen primordium emergence, to capture gene expression just after *STS1* expression is turned on (6). Because genetic diversity is high in maize, we compared expression profiles within genetic backgrounds to control for differences that could arise because of incomplete introgression of the *STS1* transgenes (21, 22). We measured differential expression by comparing expression in each line (*STS1-HOM* and *STS1-HET*) against expression in their mutant siblings.

These analyses revealed more differentially expressed genes in *STS1-HOM* than in *STS1-HET*, as compared to mutant siblings. At a 5% false discovery rate (FDR), there were 501 differentially expressed genes in inflorescences expressing *STS1-HET,* as compared to *sts1* mutant siblings (Fig. 2A). In inflorescences expressing *STS1-HOM*, we found 1,257 differentially expressed genes, as compared to *sts1* mutant siblings (Fig. 2B). There were also 109 shared genes differentially regulated by both *STS1-HOM* and *STS1-HET*. STS1-HOM can both homodimerize and heterodimerize with SI1 (18). Therefore, to see how gene expression was affected specifically by the STS1 homodimer, we compared gene expression between inflorescences expressing either *STS1-HET* or *STS1-HOM*, in a *si1* mutant background. We found that only 5 genes were differentially expressed in *STS1-HET* inflorescences, as compared to *si1* mutant siblings (Fig. 2C). In contrast, in inflorescences expressing *STS1-HOM*, 91 genes were

differentially expressed, as compared to *si1* mutant siblings (Fig. 2D). These contrasts indicate that B-class dimerization affects patterns of gene expression in developing inflorescences, either directly or indirectly.

To determine whether the genes regulated by STS1-HET and STS1-HOM were qualitatively similar, we performed GO-term analyses with our differentially expressed gene sets, in an *sts1* mutant background (Tables S2 and S3). To compare these lists of enriched GO-terms, we used GO-correlation plots (23) (Fig. 2E-F). Since the *STS1-HET* and *STS1-HOM* constructs were so similar, and since our morphological data suggested very subtle functional differences between *STS1-HET* and *STS1-HOM* (Fig. 1), we reasoned that *STS1-HET* and *STS1-HOM* were regulating similar processes. Therefore, we made the threshold for calling a GO-term unique to either dataset very stringent; only GO-terms with an enrichment p-value of less than 0.01 in one dataset, and an enrichment p-value of more than 0.25 in the other dataset were called 'unique' (Fig. 2E, sectors i and v). Using these comparisons, we found many GO-terms related to development shared between *STS1-HET* and *STS1-HOM* (Figure 2E). Indeed, 29 of the 65 enriched GO-terms shared between *STS1-HET* and *STS1-HOM* were related to development (p-value in both datasets <0.01, Fig. 1E, sector iii). GO-terms related to signaling and metabolism were also enriched in both datasets, although more of these terms were specifically enriched in *STS1-HOM*. The most highly enriched GO-terms in *STS1-HOM* were not significantly enriched in *STS1-HET* (p-value > 0.25). These GO-terms, specific to *STS1-HOM*, were almost all related to chromatin assembly and protein modification (Fig. 2E, sector i). Thus, core floral developmental programs were activated in inflorescences expressing *STS1-HOM*, but B-class dimerization also affected the expression of unique sets of genes, particularly genes involved in chromatin assembly and remodeling.

**A complex of B-, C- and E-class proteins is conserved in maize**

Differential dimerization could affect the composition of protein complexes, which is crucial for MADS-box function (3, 4). To determine which proteins interacted with STS1-HET vs. STS1-HOM, we performed immunoprecipitations (IPs) of STS1-HET and STS1-HOM in an *sts1* mutant background, using a specific antibody against GFP (ChromoTek). We analyzed precipitated complexes using quantitative mass spectrometry (MS). After confirming the presence of STS1 in the IP complex through immunoblotting (Fig. S3A-B), we performed trypsin digestion and LC-MS/MS followed by label-free protein quantification (24). The *sts1* mutant was used as a negative control to detect non-specific proteins in the mass spectrometry analysis. The iBAQ (intensity Based Absolute Quantification) method was used to compare the abundances of identified proteins (25–27). Protein identification was based on at least 5 exclusive peptides and two replicates were performed for each sample; protein abundances were similar between replicates (Fig. S3 C-D). We found a higher number of proteins in complex with STS1-HOM; 451 proteins were either specific to STS1-HOM, or were at least 2 fold higher than in mutant siblings (Dataset S9). In contrast, we found 414 proteins in complex with STS1-HET, with the same parameters (Dataset S10).

The first set of proteins in our immunoprecipitations that we explored were the MADS-box proteins. Ancestral protein resurrection and *in vitro* surveys of protein-protein interactions predict that complexes of B-, C-, and E-class MADS-box proteins are conserved across flowering plants (4, 11, 28). However, this prediction remains largely untested *in planta*, especially in monocots. Therefore, we specifically searched for other MADS-box proteins in our IP-MS data. In the STS1-HET IP-MS results, we found both STS1 and SI1 peptides, as well as peptides for three E-class MADS-box proteins (ZmMADS27, ZmMADS7, ZmMADS6), one C-class protein (an AGAMOUS (AG) homolog, ZAG1) and one D-class protein (an AGL5 homolog, ZAG4) (29, 30, Table S4). In STS1-HOM, we found the same three E-class proteins and the C-class protein ZAG1, but did not find AGL5. AGL5 was identified as one of the most enriched proteins in the STS1-HET IP, and was the only MADS-box protein specific to STS1-HET. Homologs of AGL5 are involved in gynoecium and ovule development in *A. thaliana* and rice, and AGL5 is a direct target of AGAMOUS (29–31). The AGL5 *A. thaliana* homolog, SHATTERPROOF2, is

found in complex with AG, but has not been found in complex with PISTILLATA (32). This suggests differences in B-class complexes between *A. thaliana* and maize. However, our results are consistent with broad conservation of B-, C-, and E-class protein complexes (4, 12).

**B-class dimerization affected protein abundance**

Except for SI1, the MADS-box proteins that we identified in both IP datasets were at much higher levels in STS1-HOM than in STS1-HET. This included STS1-HOM itself: absolute iBAQ values for STS1-HOM were 4.0 times higher than for STS1-HET, 3.58 times higher normalized to SI1 (Fig. 3B and S3 C-D). The higher abundance of STS1-HOM in our immunoprecipitations could have been due to complex stoichiometry, where STS1-HOM homodimerization increased because of double the number of STS1-HOM proteins in MADS-box complexes. STS1-HOM protein levels could also have been generally higher in developing flowers. We suspected higher values overall because our immunolocalizations suggested a higher abundance of STS1-HOM vs. STS1-HET, despite the same experimental conditions (Fig. S1). Because immunolocalizations are not quantitative, we carried out semi-quantitative immunoblots using a polyclonal antibody against STS1 in STS1-HOM vs. STS1-HET inflorescence tissue. In these blots, STS1-HOM was seven times more abundant than STS1-HET (Fig. 3C, Table S7). Together with our IP-MS results, these data indicate that STS1-HOM accumulated to a higher abundance than STS1-HET in inflorescence tissue.

This unexpected protein level difference led us to explore what mechanism could be responsible. STS1-HOM protein could be more abundant than STS1-HET protein because *STS1-HOM* is expressed at higher levels than *STS1-HET*. To test for this possibility, we carried out RT-qPCR using specific primers for *STS1* and *SI1* in *sts1* mutants complemented with either *STS1-HET* or *STS1-HOM*. We found that *SI1* was expressed to the same level in both lines; however, the expression of *STS1* in *STS1-HET* was 3.7 fold higher than in *STS1-HOM* (relative to actin, Fig. 3D). Similarly, in our RNA-Seq results, normalized *STS1-HET* expression was consistently double normalized *STS1-HOM* expression; approximately 15,000 counts vs. 8,600 counts respectively. Thus, despite relatively low *STS1-HOM* expression, STS1-HOM protein accumulates to higher levels than STS1-HET in floral tissue. This suggests that STS1 homodimerization lead to increased protein accumulation independent of RNA levels.

The other MADS-box proteins that we detected in our immunoprecipitations were also more abundant in STS1-HOM than in STS1-HET. ZAG1, ZmMADS6 and ZmMADS7 increased in abundance 2- to 9-fold in STS1-HOM, as compared to STS1-HET (Fig. 3B). As with STS1-HOM, higher amounts of ZAG1, ZmMADS6, ZmMADS7, and ZmMADS27 could have been because of differences in protein complex assembly or persistence in the presence of STS1-HET vs. STS1-HOM. Alternatively, the genes encoding these proteins could have been upregulated by STS1-HOM, resulting in higher protein abundance. To distinguish between these possibilities, we looked for these genes in our RNA-Seq data, and found that they were not differentially expressed between *STS1-HOM* and their mutant siblings. From all the identified MADS-box proteins, SI1 was the only one found at similar levels in both STS1-HET and STS1-HOM immunoprecipitations. This suggests that SI1 is able to compete with STS1-HOM to form heterodimers and that SI1 may be a limiting factor in MADS-box protein complex assembly. Taken together, our results show that STS1 homodimerization is either directly affecting the assembly of MADS-box complexes, or indirectly affecting complex persistence because of its higher abundance.

**STS1-HET and STS1-HOM form complexes with chromatin remodelers, kinases and the ubiquitylation machinery**

To explore our IP-MS datasets further, we performed GO-term enrichment analyses with identified proteins in the STS1-HET vs. STS1-HOM immunoprecipitations. In these analyses, we only included proteins with at least a two-fold change as compared to *sts1* siblings. When we compared the resulting lists of enriched GO-terms, our results were similar to the RNA-Seq comparisons: development, signaling, and metabolism-related GO-terms were enriched in both datasets to varying degrees. However,

chromatin-related GO-terms were no longer exclusively enriched in the STS1-HOM dataset (Fig. 2E, 3A, S4, Tables S5 and S6).

We found GO-categories related to chromatin modification enriched in both the STS1-HOM and the STS1-HET immunoprecipitation (Fig. 3A). One specific protein related to chromatin modification was the ISWI chromatin-remodeling complex ATPase CHR11 (Gene ID Zm00001d040831), which we found in complex with both STS1-HET and STS1-HOM. One protein we found only in the STS1-HOM immunoprecipitation was a FRIGIDA-like protein (Zm00001d039594). In *A. thaliana*, FRIGIDA functions as a scaffold for recruiting chromatin modification factors (33). MADS-box proteins have long been known to associate with the chromatin remodeling machinery in *A. thaliana*, including with a homolog of CHR11 (32, 34). Our results show that this may also be the case in maize, and that B-class dimerization may impact associated transcriptional dynamics.

We also found a class of proteins related to signaling in our immunoprecipitation datasets, specifically kinases. We found that ten kinases were immunoprecipitated with STS1-HET, and eleven with STS1-HOM; only two of these were in both samples. Interestingly, the kinases found with STS1-HET were related to basal metabolism, for example a phosphoglycerate kinase (Zm00001d015376) and a pyruvate kinase (Zm00001d023379), involved in synthesis and degradation of carbohydrates (35, 36). In contrast, the kinases that immunoprecipitated with STS1-HOM were related to signaling and membrane receptors; for example BR-signaling kinase 2 (Zm00001d030021) and BR-LRR receptor kinase (Zm00001d052323) (37, 38). However, further analyses are necessary to confirm interaction of STS1 with these kinases.
One new set of GO-terms that emerged in our analysis was related to protein modification and ubiquitylation. These GO-terms were more enriched in STS1-HOM, but were still present in STS1-HET (Fig. 3A). When we explored which proteins might be represented by these enriched GO-terms, we found five proteins of the Cul4-RING E3 ubiquitin ligase complex (CAND1, CUL1, CUL4, XPO1A and CDC) in the STS1-HOM IP, two of which (CAND1 and CUL1) were also in with STS1-HET IP. These proteins are in the same complex in other species, which gives us additional confidence in our IP results (39–41). However, they have not been reported as MADS-box interactors. Thus, our IP-MS results indicate that MADS-box complexes in maize may interact with the ubiquitylation machinery.

**STS1 is post-translationally modified**

The presence of kinases and ubiquitylation machinery in our IP results suggested that the higher abundance of STS1-HOM may have been regulated at the protein level by posttranslational modifications. Therefore, we explored the phosphorylation and ubiquitylation of STS1-HET vs. STS1-HOM. To do this, we performed immunoblots using commercial Anti-pSer and Anti-Ubiquitin monoclonal antibodies (Santa Cruz Biotechnology). We found that both STS1-HET and STS1-HOM proteins were phosphorylated (Fig. 3E). When we analyzed IP complexes with an Anti-Ubiquitin antibody, we identified ubiquitylated proteins in both the STS1-HET and the STS1-HOM complex. We found no differences in phosphorylation or ubiquitylation between STS1-HET and STS1-HOM using these two assays (Fig. 3E). This indicates that STS1-HET and STS1-HOM are both phosphorylated and in complex with ubiquitylated proteins, and also suggests that the higher abundance of STS1-HOM is not because it is differentially phosphorylated or ubiquitylated. Instead, the higher abundance of STS1-HOM may have allowed us to detect interactions between B-class proteins and the ubiquitylation and phosphorylation machinery that might otherwise have gone unnoticed.

**Discussion**

Here, we show that floral development in maize is robust to an evolutionary shift in B-class MADS-box protein-protein interactions. This robustness is predicted by network analyses of MADS-box protein-protein interactions, and may be important in the evolution of floral form (28). Very few MADS-box protein-protein interactions have been examined in a comparative framework. However, given evolutionary variation in interactions between B-class proteins (the least promiscuous of the floral

MADS-box proteins); the propensity for rapid evolution of MADS-box protein-protein interactions; and many lineage-specific MADS-box gene duplications, MADS-box protein-protein interactions profiles are likely diverse within populations and species (18, 42–45). This cryptic molecular diversity may contribute to the overall evolvability of floral morphology; when genetic variation can accumulate in a system, without consequent phenotypic change, the system itself can be more evolvable (46). Indeed, morphological floral traits like the lengths of stamens, stigmas, and corolla tubes are evolvable, and can change under selection after only short periods of time (47–49). Selection on floral form may also not be limited by genetic variation, indicating underlying variation in the genetic networks that regulate flower development (50). Variation in MADS-box protein-protein interaction networks may represent some of that genetic variation - acting as grist for the mill of natural selection.

MADS-box genes can regulate both complex suites of traits, like organ identity, and individual organ traits, like organ size (19) We found that variation in B-class MADS-box dimerization could affect one aspect of anther shape, namely aspect ratio. Subtle variation in anther shape can impact pollination biology. For example, in the eudicots *Plantago* and *Thalictrum,* anther properties are important in efficient pollen release from anthers (51–53). In *Primula*, another eudicot, variation in anther height is critical in the evolution of heterostyly. Interestingly, a homolog of *STS1* may underlie this height variation (54). In maize, and likely also in *Primula,* genetics using null mutant phenotypes would have obscured roles for master regulators like the B-class genes in the development of individual organ traits. In contrast, dissecting the evolutionary consequences of small changes in gene sequence can reveal specific functions for pleiotropic genes. This is critical in this era of genome editing, where the technical ability to edit specific DNA base-pairs exists, but the fundamental knowledge of exactly which base-pairs to edit is lacking.

We found both C-class and E-class MADS-box proteins interacting with both STS1-HET and STS1-HOM in our IP experiments. Homologs of these proteins have also been found in the *A. thaliana* PISTILLATA protein complex (32), indicating that complexes of B, C and E-class MADS-box proteins are conserved in maize, as predicted by models of floral development and evolution (4, 12, 13). Various models have been proposed to explain genetic interactions in monocot floral development. In oil palm, for example, there is a clear distinction between sepals and petals and the eudicot ABCE model may be conserved (55). But, in the Liliales and Asparagales, where sepals and petals are very similar, a modified ABC model was proposed (56, 57). The BCE-complexes we identified suggest that interactions in maize could be explained by the eudicot ABCE model. However, most information about MADS-box interactions comes from genetic analyses and yeast two hybrid assays. Before our work, *in vivo* MADS-box protein-protein interactions had only been shown in *A. thaliana* (32, 58). In the future, analyses of MADS-box complex formation in a comparative framework are essential for revealing both conserved and divergent aspects of the molecular biology underlying floral development.

The evolution of MADS-box complex assembly has long been considered only in terms of combinatorial complex assembly. Our results show that evolutionary variability in MADS-box complexes may also affect protein degradation dynamics. Our data suggests that complexes containing STS1 are ubiquitylated and degraded in the proteasome, and that B-class dimerization may affect the dynamics of this degradation. This variable degradation could affect the spectrum of MADS-box complexes present at any one time and, in turn, downstream gene regulation and floral development (12). In *A. thaliana,* MADS-box proteins are degraded as a result of interactions with effector proteins from phytoplasma pathogens (59–61). Some phytoplasma effectors have evolved convergently to resemble the protein-protein interaction domains of MADS-box proteins (62, 63). Interactions between MADS-box proteins and these MADS-resembling effectors are likely critical in shuttling MADS-box proteins to the proteasome under phytoplasma infection (59, 61, 62). Our results suggest that phytoplasma effectors may be hijacking a natural process where MADS-box proteins are ubiquitylated and degraded. The effect of MADS-box

complex assembly on protein degradation that we uncovered reveals an additional layer of complexity in the evolution of floral development.

**Materials and Methods**

Experimental details, including materials, methods, and data analyses are provided in the Supporting Information. Raw sequencing data is available at NCBI SRA (link to follow). Supplemental datasets and anther images are available as a dryad data repository (link to follow). Code for analyses and figure generation is available on GitHub (link to follow).

**Acknowledgements**

The authors acknowledge Genomics Resource Laboratory for genomics services and the Light Microscopy Facility and Nikon Center of Excellence at the Institute for Applied Life Sciences, University of Massachusetts Amherst with support from the Massachusetts Life Sciences Center. The authors also acknowledge the staff at the University of Massachusetts Amherst College of Natural Sciences greenhouse, the staff at the UMass crop and animal research and education farm in South Deerfield, high school intern Amanda Dee, and UMass Amherst undergraduates Michelle Heeney, Jeff Heithmar, and Grace Pisano.

**Author Contributions**

MB, CW, AS-L and MJAJ designed the research. AS-L, MJAJ, MB, CB and JM conducted research and analysed results. MB and PH acquired funding for the research. MB, MJAJ, and AS-L wrote the paper with assistance from co-authors.

**Figure Legends**

**Figure 1.** B-class dimerization has subtle effects on floral development in maize. (**A**) Stamen identity (marked with *) is lost in both (**B**) *sts1* (**C**) and *si1* mutant flowers. At anthesis, *sts1* mutant flowers complemented with either the (**D**) STS1-HET or (**E**) STS1-HOM transgene are resemble wild type flowers and each other. (**F**) The STS1-HOM transgene did not rescue the *si1* mutant phenotype. (**G-J**) Confocal microscopy showing localization of (**G-H**) STS1-HET and (**I-J**) STS1-HOM localization in developing flowers. Dotted lines in H and J indicate developing gynoecia, numbers in upper right corner indicate frequencies at which we observed the shown localization patterns. (**K-N**) Anther shape metrics (**K-L)** during development and (**M-N**) at anthesis. (**K**) During development, anther aspect ratio (AR) (anther width/anther length) was higher in STS1-HOM anthers than in STS1-HET anthers (p-value = p-value = 6.8e-10, left), while anther area (anther width*anther length) was not significantly different (p-value = 0.2592, right). (**L**) Confocal images of developing anthers measured in (**K**). (**M**) At anthesis, anther AR is lower in STS1-HOM anthers than in STS1-HET anthers (p-value = 0.003, left), while anther area (anther width*anther length) is not significantly different (p-value = 0.367, right). p-values calculated using Student's t-test. (**N**) 25 randomly selected anthers from the first (bottom) and fourth (top) quartiles of anthers measured in (**M**), colored according to *STS1* transgene genotype.

**Figure 2.** B-class dimerization affects transcriptional profiles in developing tassel flowers. (**A-B**) Differential gene expression in *sts1* mutants complemented with either the (**A**) *STS1-HET* or (**B**) *STS1-HOM* transgene, as compared to *sts1* mutant siblings. (**C-D**) Differential gene expression in *si1* mutants complemented with either the (**C**) *STS1-HET* (**D**) or *STS1-HOM* transgene, as compared to *si1* mutant siblings. (**E**) GO-term correlation plots comparing probabilities of GO-term enrichments in STS1-HET and STS1-HOM. Left panel shows all GO-terms, right panel excludes highly enriched GO-terms in *STS1-HOM*. Dot sizes are proportional to the number of genes in each enriched GO-term category, and colored according to which larger category they are associated with. P-value cutoffs for sectors: (i) p-value x > 0.25 & p-value y < 0.01; (ii) 0.01 < p-value x < 0.25 & p.value y < 0.01; (iii) p-value x < 0.01 & p-value y < 0.01; (iv) p.value x < 0.01 & 0.01 < p-value y < 0.25; (v) p-value x < 0.01 & p-value x > 0.25.

**Figure 3.** B-class dimerization affects protein abundance and protein complex assembly in developing tassel flowers. (**A**) GO-term correlation plot comparing probabilities of GO-term enrichments in the STS1-HET vs. STS1-HOM IP-MS datasets. Dot sizes are proportional to the number of genes in each enriched GO-term category, and colored according to which larger category they are associated with. (**B**) Relative abundances of MADS-box proteins in the IP-MS datasets. STS1, as well as C-class and E-class proteins are higher in STS1-HOM than in STS1-HET immunoprecipitations. (**C**) Semi-quantitative immunoblots with anti-STS1 (top) and anti-TUBULIN (bottom) also show that STS1-HET is less abundant than STS1-HOM. (**D**) RT-qPCR shows that *STS1-HET* RNA is more abundant than than *STS1-HOM* RNA, relative to actin. *SI1* RNA occurs at similar levels, relative to actin, in both STS1-HET and STS1-HOM inflorescences. (**E**) STS1-HET and STS1-HOM are phosphorylated, and in complex with ubiquitylated proteins. p-value cutoffs for sectors in GO-correlation plot: (i) p-value x > 0.25 & p-value y < 0.01; (ii) 0.01 < p-value x < 0.25 & p.value y < 0.01; (iii) p-value x < 0.01 & p-value y < 0.01; (iv) p.value x < 0.01 & 0.01 < p-value y < 0.25; (v) p-value x < 0.01 & p-value x > 0.25.

**Figures**

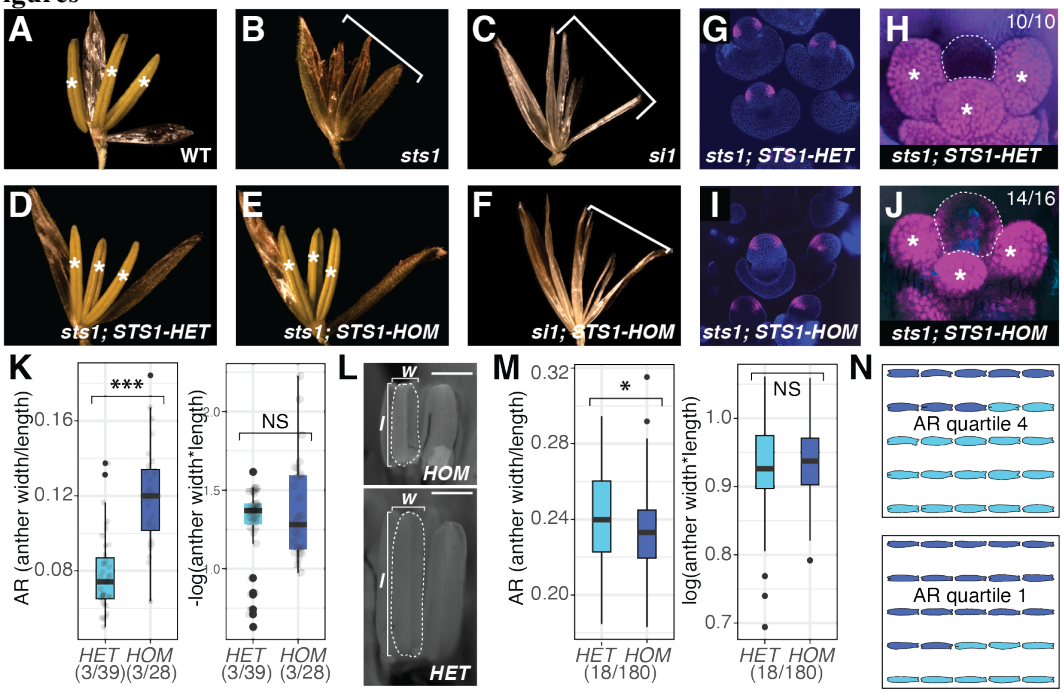


**Figure 1.** B-class dimerization has subtle effects on floral development in maize. (**A**) Stamen identity (marked with *) is lost in both (**B**) *sts1* (**C**) and *si1* mutant flowers. At anthesis, *sts1* mutant flowers complemented with either the (**D**) STS1-HET or (**E**) STS1-HOM transgene are resemble wild type flowers and each other. (**F**) The STS1-HOM transgene did not rescue the *si1* mutant phenotype. (**G-J**) Confocal microscopy showing localization of (**G-H**) STS1-HET and (**I-J**) STS1-HOM localization in developing flowers. Dotted lines in H and J indicate developing gynoecia, numbers in upper right corner indicate frequencies at which we observed the shown localization patterns. (**K-N**) Anther shape metrics (**K-L**) during development and (**M-N**) at anthesis. (**K**) During development, anther aspect ratio (AR) (anther width/anther length) was higher in STS1-HOM anthers than in STS1-HET anthers (p-value = p-value = 6.8e-10, left), while anther area (anther width*anther length) was not significantly different (p-value = 0.2592, right). (**L**) Confocal images of developing anthers measured in (**K**). (**M**) At anthesis, anther AR is lower in STS1-HOM anthers than in STS1-HET anthers (p-value = 0.003, left), while anther area (anther width*anther length) is not significantly different (p-value = 0.367, right). p-values calculated using Student's t-test. (**N**) 25 randomly selected anthers from the first (bottom) and fourth (top) quartiles of anthers measured in (**M**), colored according to *STS1* transgene genotype.

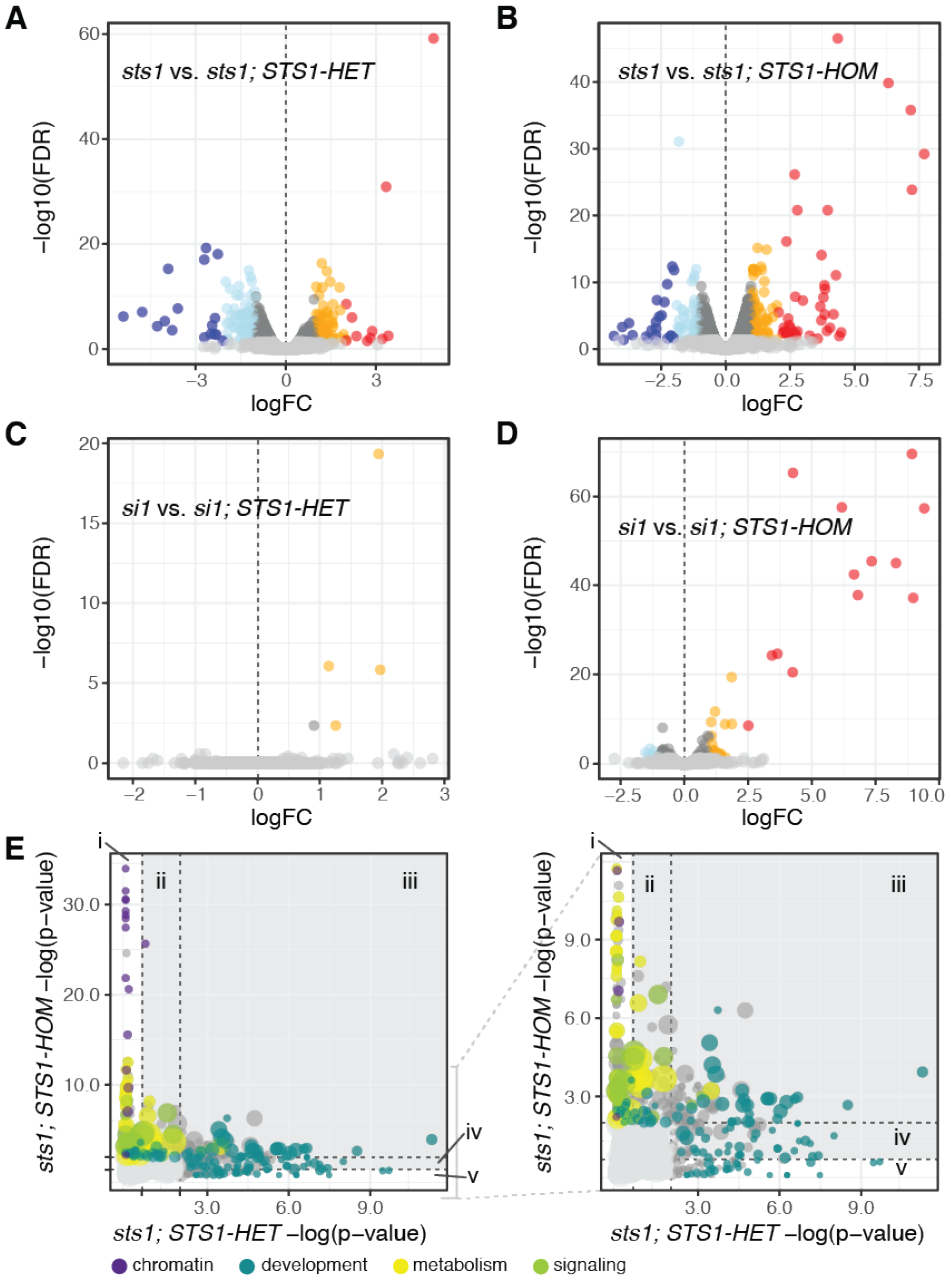


**Figure 2.** B-class dimerization affects transcriptional profiles in developing tassel flowers. (**A-B**) Differential gene expression in *sts1* mutants complemented with either the (**A**) *STS1-HET* or (**B**) *STS1-HOM* transgene, as compared to *sts1* mutant siblings. (**C-D**) Differential gene expression in *si1* mutants complemented with either the (**C**) *STS1-HET* (**D**) or *STS1-HOM* transgene, as compared to *si1* mutant siblings. (**E**) GO-term correlation plots comparing probabilities of GO-term enrichments in STS1-HET and STS1-HOM. Left panel shows all GO-terms, right panel excludes highly enriched GO-terms in *STS1-HOM*. Dot sizes are proportional to the number of genes in each enriched GO-term category, and colored according to which larger category they are associated with. P-value cutoffs for sectors: (i) p-value x > 0.25 & p-value y < 0.01; (ii) 0.01 < p-value x < 0.25 & p.value y < 0.01; (iii) p-value x < 0.01 & p-value y < 0.01; (iv) p.value x < 0.01 & 0.01 < p-value y < 0.25; (v) p-value x < 0.01 & p-value x > 0.25.

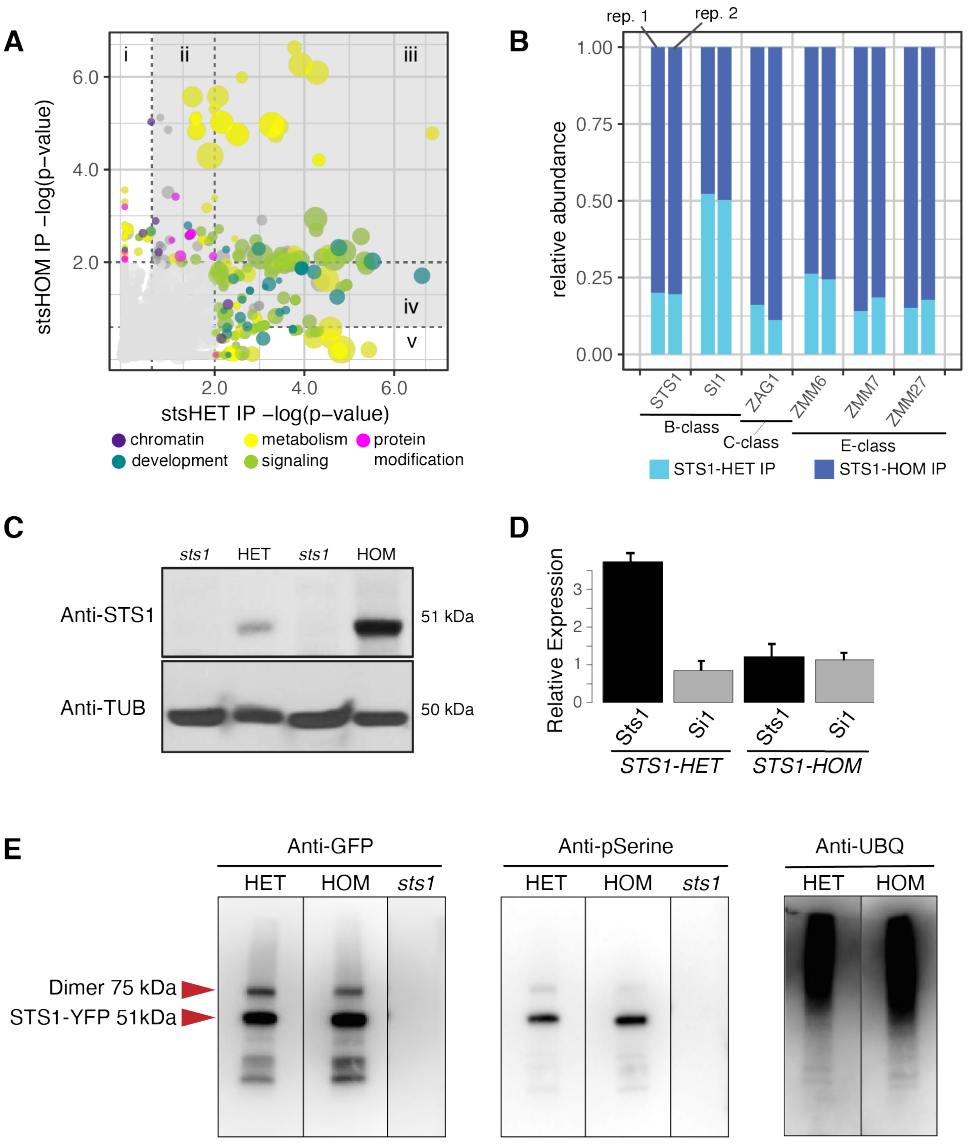


**Figure 3.** B-class dimerization affects protein abundance and protein complex assembly in developing tassel flowers. (**A**) GO-term correlation plot comparing probabilities of GO-term enrichments in the STS1-HET vs. STS1-HOM IP-MS datasets. Dot sizes are proportional to the number of genes in each enriched GO-term category, and colored according to which larger category they are associated with. (**B**) Relative abundances of MADS-box proteins in the IP-MS datasets. STS1, as well as C-class and E-class proteins are higher in STS1-HOM than in STS1-HET immunoprecipitations. (**C**) Semi-quantitative immunoblots with anti-STS1 (top) and anti-TUBULIN (bottom) also show that STS1-HET is less abundant than STS1-HOM. (**D**) RT-qPCR shows that *STS1-HET* RNA is more abundant than than *STS1-HOM* RNA, relative to actin. *SI1* RNA occurs at similar levels, relative to actin, in both STS1-HET and STS1-HOM inflorescences. (**E**) STS1-HET and STS1-HOM are phosphorylated, and in complex with ubiquitylated proteins. p-value cutoffs for sectors in GO-correlation plot: (i) p-value x > 0.25 & p-value y < 0.01; (ii) 0.01 < p-value x < 0.25 & p.value y < 0.01; (iii) p-value x < 0.01 & p-value y < 0.01; (iv) p.value x < 0.01 & 0.01 < p-value y < 0.25; (v) p-value x < 0.01 & p-value x > 0.25.

**References**


1. E. S. Coen, E. M. Meyerowitz, The War of the Whorls: Genetic Interactions Controlling Flower Development. *Nature* **353**, 31–37 (1991).
2. B. A. Krizek, J. C. Fletcher, Molecular mechanisms of flower development: an armchair guide. *Nat. Rev. Genet.* **6**, 688–698 (2005).
3. G. Theissen, H. Saedler, Plant biology. Floral quartets. *Nature* **409**, 469–471 (2001).
4. G. Theissen, R. Melzer, F. Rümpler, MADS-domain transcription factors and the floral quartet model of flower development: linking plant development and evolution. *Development* **143**, 3259–3271 (2016).
5. E. M. Kramer, Plus ça change, plus c'est la même chose: The developmental evolution of flowers. *Current Topics in Developmental Biology*, 211–238 (2019).
6. M. E. Bartlett, *et al.*, The Maize PI/GLO Ortholog Zmm16/sterile tassel silky ear1 Interacts with the Zygomorphy and Sex Determination Pathways in Flower Development. *Plant Cell* **27**, 3081–3098 (2015).
7. B. A. Ambrose, *et al.*, Molecular and genetic analyses of the silky1 gene reveal conservation in floral organ specification between eudicots and monocots. *Mol. Cell* **5**, 569–579 (2000).
8. K. Goto, E. M. Meyerowitz, Function and regulation of the Arabidopsis floral homeotic gene PISTILLATA. *Genes and Development* **8**, 1548–1560 (1994).
9. B. A. Krizek, E. M. Meyerowitz, The Arabidopsis homeotic gene APETALA3 and PISTILLATA are sufficient to provide the B class organ identity function. *Development* **122**, 11–22 (1996).
10. N. Nagasawa, *et al.*, SUPERWOMAN1 and DROOPING LEAF genes control floral organ identity in rice. *Development* **130**, 705–718 (2003).
11. A. S. Veron, K. Kaufmann, E. Bornberg-Bauer, Evidence of interaction network evolution by whole-genome duplications: A case study in MADS-box proteins. *Mol. Biol. Evol.* **24**, 670–678 (2007).
12. P. Ruelens, *et al.*, The origin of floral organ identity quartets. *Plant Cell* **29**, 229–242 (2017).
13. M. Mondragon-Palomino, G. Theissen, MADS about the evolution of orchid flowers. *Trends Plant Sci.* **13**, 51–59 (2008).
14. H.-F. Hsu, *et al.*, Model for perianth formation in orchids. *Nature Plants* **1**, 15046 (2015).
15. C. D. Specht, M. E. Bartlett, Flower Evolution: The Origin and Subsequent Diversification of the Angiosperm Flower. *Annu. Rev. Ecol. Evol. Syst.* **40**, 217–243 (2009).
16. Y.-Q. Wang, R. Melzer, G. Theissen, Molecular interactions of orthologues of floral homeotic proteins from the gymnosperm Gnetum gnemon provide a clue to the evolutionary origin of "floral quartets." *Plant J.* **64**, 177–190 (2010).
17. C. J. Whipple, *et al.*, Conservation of B-class floral homeotic gene function between maize and Arabidopsis. *Development* **131**, 6083–6091 (2004).
18. M. Bartlett, *et al.*, Evolutionary Dynamics of Floral Homeotic Transcription Factor Protein–Protein Interactions. *Mol. Biol. Evol.* **33**, 1486–1501 (2016).
19. S. E. Wuest, *et al.*, Molecular basis for the specification of floral organs by APETALA3 and PISTILLATA. *Proc. Natl. Acad. Sci. U. S. A.* **109** (2012).
20. V. Bonhomme, S. Picq, C. Gaucherel, J. Claude, Others, Momocs: outline analysis using R. *J. Stat. Softw.* **56**, 1–24 (2014).
21. E. S. Buckler, B. S. Gaut, M. D. McMullen, Molecular and functional diversity of maize. *Curr. Opin. Plant Biol.* **9**, 172–176 (2006).
22. W. Zhao, *et al.*, Panzea: a database and resource for molecular and functional diversity in the maize genome. *Nucleic Acids Res.* **34**, D752–7 (2006).
23. C. M. Bergey, *et al.*, Polygenic adaptation and convergent evolution on growth and cardiac genetic pathways in African and Asian rainforest hunter-gatherers. *Proc. Natl. Acad. Sci. U. S. A.* **115**, E11256–E11263 (2018).
24. P. Sinitcyn, J. D. Rudolph, J. Cox, Computational Methods for Understanding Mass Spectrometry–Based Shotgun Proteomics Data. *Annu. Rev. Biomed. Data Sci.* **1**, 207–234 (2018).
25. B. Schwanhäusser, *et al.*, Global quantification of mammalian gene expression control. *Nature* **473**,

337–342 (2011).
26. B. He, J. Shi, X. Wang, H. Jiang, H.-J. Zhu, Label-free absolute protein quantification with data-independent acquisition. *J. Proteomics* **200**, 51–59 (2019).
27. J. F. Krey, *et al.*, Accurate label-free protein quantitation with high- and low-resolution mass spectrometers. *J. Proteome Res.* **13**, 1034–1044 (2014).
28. Z. Zhang, *et al.*, Resurrected Protein Interaction Networks Reveal the Innovation Potential of Ancient Whole-Genome Duplication. *The Plant Cell* **30**, 2741–2760 (2018).
29. L. Dreni, *et al.*, The D-lineage MADS-box gene OsMADS13 controls ovule identity in rice. *Plant J.* **52**, 690–699 (2007).
30. S. J. Liljegren, *et al.*, SHATTERPROOF MADS-box genes control seed dispersal in Arabidopsis. *Nature* **404**, 766–770 (2000).
31. M. Colombo, *et al.*, A new role for the SHATTERPROOF genes during Arabidopsis gynoecium development. *Dev. Biol.* **337**, 294–302 (2010).
32. C. Smaczniak, *et al.*, Characterization of MADS-domain transcription factor complexes in arabidopsis flower development. *Proc. Natl. Acad. Sci. U. S. A.* **109**, 1560–1565 (2012).
33. X. Hu, *et al.*, Proteasome-mediated degradation of FRIGIDA modulates flowering time in Arabidopsis during vernalization. *Plant Cell* **26**, 4763–4781 (2014).
34. G. Vachon, J. Engelhorn, C. C. Carles, Interactions between transcription factors and chromatin regulators in the control of flower development. *J. Exp. Bot.* **69**, 2461–2471 (2018).
35. S. Rosa-Téllez, *et al.*, Phosphoglycerate Kinases Are Co-Regulated to Adjust Metabolism and to Optimize Growth. *Plant Physiol.* **176**, 1182–1198 (2018).
36. Z. Lu, T. Hunter, Metabolic Kinases Moonlighting as Protein Kinases. *Trends Biochem. Sci.* **43**, 301–310 (2018).
37. W. Tang, *et al.*, BSKs Mediate Signal Transduction from the Receptor Kinase BRI1 in Arabidopsis. *Science* **321**, 557–560 (2008).
38. P. Xu, *et al.*, A brassinosteroid-signaling kinase interacts with multiple receptor-like kinases in Arabidopsis. *Mol. Plant* **7**, 441–444 (2014).
39. S. Feng, *et al.*, Arabidopsis CAND1, an unmodified CUL1-interacting protein, is involved in multiple developmental pathways controlled by ubiquitin/proteasome-mediated protein degradation. *Plant Cell* **16**, 1870–1882 (2004).
40. I. E. Wertz, *et al.*, Human De-etiolated-1 regulates c-Jun by assembling a CUL4A ubiquitin ligase. *Science* **303**, 1371–1374 (2004).
41. K. K. Adhvaryu, *et al.*, The cullin-4 complex DCDC does not require E3 ubiquitin ligase elements to control heterochromatin in Neurospora crassa. *Eukaryot. Cell* **14**, 25–28 (2015).
42. C. S. Silva, *et al.*, Evolution of the Plant Reproduction Master Regulators LFY and the MADS Transcription Factors: The Role of Protein Structure in the Evolutionary Development of the Flower. *Front. Plant Sci.* **6**, 1193 (2015).
43. R. Melzer, *et al.*, DEF-and GLO-like proteins may have lost most of their interaction partners during angiosperm evolution. *Ann. Bot.*, mcu094 (2014).
44. S. Soyk, *et al.*, Bypassing Negative Epistasis on Yield in Tomato Imposed by a Domestication Gene. *Cell* **169**, 1142–1155.e12 (2017).
45. T. Alhindi, *et al.*, Protein interaction evolution from promiscuity to specificity with reduced flexibility in an increasingly complex network. *Sci. Rep.* **7**, 44948 (2017).
46. A. Wagner, The role of robustness in phenotypic adaptation and innovation. *Proc. Biol. Sci.* **279**, 1249–1258 (2012).
47. Ø. H. Opedal, The evolvability of animal-pollinated flowers: towards predicting adaptation to novel pollinator communities. *New Phytol.* **221**, 1128–1135 (2019).
48. Ø. H. Opedal, G. H. Bolstad, T. F. Hansen, W. S. Armbruster, C. Pélabon, The evolvability of herkogamy: Quantifying the evolutionary potential of a composite trait. *Evolution* **71**, 1572–1586 (2017).
49. J. K. Conner, *et al.*, Rapid independent trait evolution despite a strong pleiotropic genetic correlation.

*Am. Nat.* **178**, 429–441 (2011).
50. T. L. Ashman, C. J. Majetic, Genetic constraints on floral evolution: a review and evaluation of patterns. *Heredity* **96**, 343–352 (2006).
51. D. Timerman, S. C. H. Barrett, Comparative analysis of pollen release biomechanics in Thalictrum: implications for evolutionary transitions between animal and wind pollination. *New Phytol.* **224**, 1121–1132 (2019).
52. D. Timerman, S. C. H. Barrett, Divergent selection on the biomechanical properties of stamens under wind and insect pollination. *Proc. Biol. Sci.* **285**, 20182251 (2018).
53. D. Timerman, D. F. Greene, J. Urzay, J. D. Ackerman, Turbulence-induced resonance vibrations cause pollen release in wind-pollinated Plantago lanceolata L. (Plantaginaceae). *J. R. Soc. Interface* **11**, 20140866 (2014).
54. J. Li, *et al.*, Genetic architecture and evolution of the S locus supergene in Primula vulgaris. *Nature Plants* **2**, 16188 (2016).
55. H. Adam, *et al.*, Functional characterization of MADS box genes involved in the determination of oil palm flower structure. *J. Exp. Bot.* **58**, 1245–1259 (2007).
56. A. Kanno, H. Saeki, T. Kameya, H. Saedler, G. Theissen, Heterotopic expression of class B floral homeotic genes supports a modified ABC model for tulip (Tulipa gesneriana). *Plant Mol. Biol.* **52**, 831–841 (2003).
57. T. Nakamura, *et al.*, The modified ABC model explains the development of the petaloid perianth of Agapanthus praecox ssp orientalis (Agapanthaceae) flowers. *Plant Mol. Biol.* **58**, 435–445 (2005).
58. J. L. Riechmann, B. A. Krizek, E. M. Meyerowitz, Dimerization specificity of Arabidopsis MADS domain homeotic proteins APETALA1, APETALA3, PISTILLATA, and AGAMOUS. *Proceedings of the National Academy of Sciences* **93**, 4793–4798 (1996).
59. A. M. MacLean, *et al.*, Phytoplasma effector SAP54 hijacks plant reproduction by degrading MADS-box proteins and promotes insect colonization in a RAD23-dependent manner. *PLoS Biol.* **12**, e1001835 (2014).
60. K. Maejima, *et al.*, Recognition of floral homeotic MADS domain transcription factors by a phytoplasmal effector, phyllogen, induces phyllody. *Plant J.* **78**, 541–554 (2014).
61. Y. Kitazawa, *et al.*, Phytoplasma-conserved phyllogen proteins induce phyllody across the Plantae by degrading floral MADS domain proteins. *J. Exp. Bot.* **68**, 2799–2811 (2017).
62. M.-B. Aurin, M. Haupt, M. Görlach, F. Rümpler, G. Theißen, Structural requirements of the phytoplasma effector protein SAP54 for causing homeotic transformation of floral organs. *bioRxiv*, 772699 (2019).
63. F. Rümpler, L. Gramzow, G. Theißen, R. Melzer, Did Convergent Protein Evolution Enable Phytoplasmas to Generate "Zombie Plants"? *Trends Plant Sci.* **20**, 798–806 (2015).

**Supporting Information**

**Materials and Methods**

*Transgenic lines and plant growth. STS1* transgenes, in the pTF101 vector backbone, were transformed into the Hi-II genetic background at the Iowa State University plant transformation facility. *STS1-HET* and *STS1-HOM* transformants were crossed to either *sts1* or *si1* mutants in the A619 genetic background. Resulting progeny carrying a transgene were identified by their ability to resist herbicide application, and crossed again to *sts1* or *si1* mutants in the A619 genetic background. Once generated, plants for all molecular analyses were grown in the UMass College of Natural Science greenhouse using a 50:50 soil mix of LC1 (SunGro Horticulture) and Turface (Turface Inc.). Field grown plants were grown at the University of Massachusetts UMass Crop and Animal Research and Education Farm in South Deerfield, MA.

*RNAseq tissue collection and sequencing.* Plants were grown in the greenhouse as described above. Shortly after stamen primordium emergence (4-5 weeks after planting), plants were harvested and inflorescence meristems were flash frozen in liquid nitrogen. Samples were harvested at the same time of day, beginning at 3pm. Three plants per genotype were pooled to generate one biological replicate, with three biological replicates per genotype (genotyping primers in Table S8). RNA was extracted from each pooled biological replicate using a combination of Trizol (Invitrogen) and Qiagen Plant RNeasy columns including a Qiagen on-column DNase digestion. 1 µg of RNA from each biological replicate was used for RNA library preparation the NEBNext Ultra library kit per manufacturer instructions (3 libraries per genotype). Samples were barcoded using NEBNext Set 1 Multiplex Oligos for Illumina to generate libraries for single end 150 base pair sequencing. DNA sequencing was performed at Genomics Resource Laboratory, University of Massachusetts Amherst using an Illumina NextSeq500.

*Differential expression analysis.* Quality and adapter filtering were performed as a part of the Illumina pipeline. Reads were mapped to the version 4 maize genome assembly Zm-B73-REFERENCE-GRAMENE-4.0 using STAR v2.5.3a (1, 2). Mapping using STAR included default parameters for alignment and seeding, quality filtering, trimming, and removal of alignments with non-canonical splice junctions to obtain counts per gene (1). Differential expression analysis was performed using the R package RUVseq for normalization, followed by differential expression analysis with edgeR (3–5). The RUVseq pipeline included upper quartile normalization using 7,000 empirically determined control genes. These empirical control genes are the 7,000 least differentially expressed genes in the dataset as determined by the analysis pipeline. Where samples did not separate clearly by our experimental variables (e.g. genetic background), those samples were not included in the downstream DE analysis, resulting in the exclusion of one STS1-HET and one STS1-HOM library.

*Confocal microscopy*. Plants were grown in the greenhouse as described above. Shortly after stamen primordium emergence (4-5 weeks after planting), plants were harvested and meristems were stained with 5 µM SynaptoRed membrane dye (VWR 80510-682) in DMSO. The confocal image data was gathered using an A1R: Nikon A1 Resonant Scanning Confocal.

*Anther shape measurement and analysis.* For measuring anthers and counting floral organs we grew plants in the greenhouse (young anthers) or field (anthers at anthesis) as described above. To measure anthers in young flowers, plants were harvested at the inflorescence meristem stage after glume development (5-6 weeks after planting). Developing flowers were imaged using Leica CTR5500 fluorescent and Zeiss 710 confocal microscopes. Anthers were measured in 3 individuals per genotype, >6 anthers per individual. To measure anthers at anthesis, dehisced anthers were harvested from the central spike on the day that flowers first opened. Anthers with filaments attached were harvested from central spikes and scanned within an hour after dehiscing. Individual anthers were placed on a slide (flat side down) and scanned using an Epson V700 scanner. Scanned images were separated into individual

files and images made binary using ImageJ (6). Individual anther image files were read into R, and anther length and width was measured using the R package MOMOCS (7). Anther aspect ratio was calculated by dividing anther width by anther length (18 individuals per genotype, 10 anthers per individual). These aspect ratio values were log-transformed (log base 10) for normality (Shapiro-Wilk normality test, p-value = 0.66). Means of log-transformed aspect ratio values were compared using Students-t-test. For the organ counts, mature anthers were harvested from the central spike prior to dehiscence and we counted lodicules and stamens in five spikelets from five individuals (50 florets total). All anther measurements are in supplemental datasets S1 and S2.

*Immunoprecipitation.* Five grams (forty plants) of pooled maize tassels (0.5 – 1.0 cm in length) were ground in liquid nitrogen using mortar and pestle. The resulting powder was mixed with 10 mL of an extraction buffer for proteins dynamically transported between nucleus and cytosol, in native conditions (50mM Tris-HCl pH 7.5, 150 mM NaCl, 1% IGEPAL-CA-630 and 1× protease inhibitor mix). Then, extract was filtered through four layers of Miracloth, and centrifuged twice at 10 000rpm for 10 min at 4°C. Protein extract was incubated with 40 uL of GFP-trap MA bead slurry (ChromoTek), shaking for 2 h at 4°C. Beads with the bound target protein were magnetically separated and washed four times with 200 uL of ice-cold wash buffer containing 50 mM Tris pH 7.5, 150 mM NaCl, 0.1% IGEPAL-CA-630 and 1X protease inhibitor mix. Bound proteins were eluted with 40 uL of elution buffer (0.05% Bromophenol blue, 0.1M DTT, 10% Glycerol, 2% SDS, 0.05M Tris-HCl pH 6.8). 5 uL were used for immunoblot to confirm the presence of the bait protein (STS1-YFP) by standard SDS-PAGE and detection by chemiluminescence with a monoclonal Anti-GFP antibody (Mouse IgG1K, clones 7.1 and 13.1, Roche Cat. No. 11814460001) and Anti-Mouse secondary antibody HRP-conjugated (Amersham ECL GE Cat. No. 45001275). Then, 35 uL was used to run a short SDS-PAGE gel, stained with GelCode Blue Safe protein stain (Thermo Fisher scientific). Gel slices were sent for mass spectrometry analysis to UMass Medical School Mass Spectrometry facility. Two replicates were performed for each genotype.
*LC-MS/MS and label-free protein quantification.* In-gel trypsin digestion was analyzed in a quadrupole-Orbitrap hybrid mass spectrometer (Thermo Sci Q-Exactive with Waters NanoAcquity UPLC). Forty individuals of each genotype (*sts1* mutants and *sts1* mutants complemented with STS1-HET or STS1-HOM) were used for each IP experiment. When a high number of individuals is used, a lower number of technical replicates in the mass spectrometer is needed to get robust results (Jorrin-Novo et al., 2015). In this experiment the reproducibility can be observed in the high number of proteins identified in both replicates for each sample, as well as in the similar abundance of each one (Supplemental Datasets S9 - S10). For protein identification, Mascot in Proteome Discoverer 2.1.1.21 with the Uniprot_Maize database was used. For label free quantification, Scaffold version 4.8.4 was used, with 90% minimum peptide threshold, 3 peptides minimum and a peptide FDR 0.05.

*Antibody production and immunolocalization.* Anti-STS1 antibody was developed from the full-length coding sequence of *STS1* cloned into pDEST17 at the Bartlett Lab, using the protocol described in (Chuck et al., 2014) with some modifications. 6HIS-STS1 was expressed and purified from *E. coli* Rosetta strain, using denaturing conditions. 200 ug of purified protein was sent to Cocalico Biologicals, PA., where two guinea pig immunizations were performed. Serum was used for antibody affinity purification to the STS1 recombinant protein using magnetic beads (Invitrogen). Validation of antibody was carried out by immunoblot with total protein extract from *sts1* complemented lines and *sts1* mutant as a negative control. STS1 immunolocalizations were performed as previously described (Chuck et al., 2010); (Tsuda et al., 2019).

*STS1 and pSerine immunoblot*. SDS-PAGE with 12% acrylamide gel was carried out with 30 ug of protein extract from *sts1*, and STS1-HET and STS1-HOM complemented mutants. Then, semidry transfer, blocking, and incubation with 1:2000 affinity-purified Anti-STS1 guinea pig polyclonal antibody was performed. Protein was detected using chemiluminescence with 1:3000 Anti-Guinea pig secondary HRP-coupled antibody (Thermo Fisher Sci Cat No. A18769). Membrane was stripped and tubulin was

detected as a loading control by incubation with 1:25,000 Mouse monoclonal anti-TUB DM1A (Abcam). Detection was done using 1:10,000 Anti-Mouse secondary HRP-conjugated antibody (Amersham ECL GE Cat. No. 45001275). For Anti-pSerine immunoblot, PhosSTOP (Roche) was added to the protein extraction buffer and blocking was carried out with 2% BSA instead milk. Primary Anti-pSer 16B4 mouse monoclonal antibody (Santa Cruz Biotechnology) was used at 1:1000. And secondary Anti-mouse HRP-conjugated (Amersham ECL GE) at 1:3000 was used. For development, Clarity ECL reagents (BioRad) and Azure c-300 Chemiluminescent immunoblot Imaging System (Azure Biosystems) were used.

*In situ hybridization and gel shifts. sts1* and *sts1* complemented inflorescences were fixed overnight at 4°C in 4% paraformaldehyde in 1X PBS. Fixed samples were dehydrated in ethanol series and transferred into Histoclear, then were embedded in Paraplast, sectioned, and hybridized according to (Bartlett et al., 2015). Gel shifts using B-class proteins were performed as described in (8).

**Supplemental Tables**

**Table S1.** Floral organ counts

| **Genotype** | **Number of individuals** | **Florets per plant** | **Stamen number** | **Lodicule number** |
|---|---|---|---|---|
| STS1-HET | 5 | 5 | 2.95 +/- 0.39 | 2.00 +/- 0 |
| STS1-HOM | 5 | 5 | 2.98 +/-0.22 | 2.05 +/- 0.2 |
| | | | NS P=0.57 | NS P=0.08 |

**Table S2.** Top 20 enriched GO-terms differentially expressed in STS1-HET vs sts1 mutant siblings

| Category | Over-represented p-value | Term |
|---|---|---|
| GO:0009908 | 5.60E-12 | flower development |
| GO:0010093 | 2.10E-10 | specification of floral organ identity |
| GO:0010092 | 3.58E-10 | specification of animal organ identity |
| GO:0048437 | 3.12E-09 | floral organ development |
| GO:0001708 | 9.99E-09 | cell fate specification |
| GO:0010254 | 3.31E-08 | nectary development |
| GO:0048467 | 3.76E-08 | gynoecium development |
| GO:0048440 | 6.18E-08 | carpel development |
| GO:0003002 | 7.21E-08 | regionalization |
| GO:0010022 | 7.46E-08 | meristem determinacy |
| GO:0007389 | 1.13E-07 | pattern specification process |
| GO:0010158 | 1.90E-07 | abaxial cell fate specification |
| GO:0010159 | 2.17E-07 | specification of animal organ position |
| GO:0010450 | 2.17E-07 | inflorescence meristem growth |
| GO:0048569 | 2.17E-07 | post-embryonic animal organ development |
| GO:0048438 | 2.80E-07 | floral whorl development |
| GO:0045165 | 2.88E-07 | cell fate commitment |
| GO:0010433 | 5.31E-07 | bract morphogenesis |
| GO:0010434 | 5.31E-07 | bract formation |
| GO:0009725 | 5.56E-07 | response to hormone |
| GO:0048367 | 6.21E-07 | shoot system development |

**Table S3.** Top 20 enriched GO-terms differentially expressed in STS1-HOM vs sts1 mutant siblings

| Category | Over-represented p-value | Term |
|---|---|---|
| GO:0000786 | 1.10E-34 | nucleosome |
| GO:0032993 | 3.23E-32 | protein-DNA complex |
| GO:0031497 | 2.70E-31 | chromatin assembly |
| GO:0006334 | 3.40E-31 | nucleosome assembly |
| GO:0065004 | 5.35E-30 | protein-DNA complex assembly |
| GO:0071824 | 1.53E-29 | protein-DNA complex subunit organization |
| GO:0034728 | 3.67E-29 | nucleosome organization |
| GO:0006323 | 3.70E-28 | DNA packaging |
| GO:0006333 | 2.31E-26 | chromatin assembly or disassembly |
| GO:0046982 | 2.57E-25 | protein heterodimerization activity |
| GO:0071103 | 1.46E-22 | DNA conformation change |
| GO:0000785 | 2.49E-21 | chromatin |
| GO:0044427 | 2.75E-16 | chromosomal part |
| GO:0044391 | 2.49E-13 | ribosomal subunit |
| GO:0071844 | 3.11E-13 | NA |
| GO:0005730 | 1.97E-12 | nucleolus |
| GO:0005694 | 2.34E-12 | chromosome |
| GO:0022626 | 8.63E-12 | cytosolic ribosome |
| GO:0022607 | 2.40E-11 | cellular component assembly |
| GO:0034622 | 7.73E-11 | cellular protein-containing complex assembly |
| GO:0034621 | 1.13E-10 | NA |

| **Table S4.** MADS-box proteins identified in IP-MS experiments | | | |
|---|---|---|---|
| **Maize Name** | **Maize ID** | **MADS Clade** | **Arabidopsis homologs** |
| STS1/ZMM16 | Zm00001d042618 | B-class | AT5G20240 |
| SILKY1 | Zm00001d036425 | B-class | AT3G54340 |
| ZMM6 | Zm00001d031620 | E-class | AT3G02310, AT2G03710, AT5G15800, AT1G24260 |
| ZMM7 | Zm00001d021057 | E-class | AT3G02310, AT2G03710, AT5G15800, AT1G24260 |
| ZMM27 | Zm00001d006094 | E-class | AT3G02310, AT2G03710, AT5G15800, AT1G24260 |
| ZAG1 | Zm00001d037737 | C-class | AT3G58780, AT4G18960, AT2G42830 |
| AGL5/ZAG4 | Zm00001d039434 | D-class | AT2G42830 AT4G18960 AT3G58780 |

**Table S5.** Top 20 enriched GO-terms in proteins immunoprecipitated with STS1-HET

| Category | Over-represented p-value | Term |
|---|---|---|
| GO:0005829 | 1.42E-07 | cytosol |
| GO:0048856 | 2.41E-07 | anatomical structure development |
| GO:0032502 | 3.07E-06 | developmental process |
| GO:0036094 | 3.68E-06 | small molecule binding |
| GO:0034641 | 4.20E-06 | cellular nitrogen compound metabolic process |
| GO:0006807 | 4.57E-06 | nitrogen compound metabolic process |
| GO:0006139 | 5.50E-06 | nucleobase-containing compound metabolic process |
| GO:0009117 | 1.15E-05 | nucleotide metabolic process |
| GO:0006753 | 1.17E-05 | nucleoside phosphate metabolic process |
| GO:0071704 | 1.30E-05 | organic substance metabolic process |
| GO:0003674 | 1.50E-05 | molecular_function |
| GO:0055086 | 1.53E-05 | nucleobase-containing small molecule metabolic process |
| GO:0000166 | 1.65E-05 | nucleotide binding |
| GO:1901265 | 1.65E-05 | nucleoside phosphate binding |
| GO:0007275 | 1.73E-05 | multicellular organism development |
| GO:0048731 | 1.86E-05 | system development |
| GO:0044237 | 2.21E-05 | cellular metabolic process |
| GO:0097159 | 2.62E-05 | organic cyclic compound binding |
| GO:0005488 | 2.66E-05 | binding |
| GO:0044707 | 2.95E-05 | NA |
| GO:0032501 | 2.97E-05 | multicellular organismal process |

**Table S6.** Top 20 enriched GO-terms in proteins immunoprecipitated with STS1-HOM

| Category | Over-represented p-value | Term |
|---|---|---|
| GO:0005829 | 1.42E-07 | cytosol |
| GO:0048856 | 2.41E-07 | anatomical structure development |
| GO:0032502 | 3.07E-06 | developmental process |
| GO:0036094 | 3.68E-06 | small molecule binding |
| GO:0034641 | 4.20E-06 | cellular nitrogen compound metabolic process |
| GO:0006807 | 4.57E-06 | nitrogen compound metabolic process |
| GO:0006139 | 5.50E-06 | nucleobase-containing compound metabolic process |
| GO:0009117 | 1.15E-05 | nucleotide metabolic process |
| GO:0006753 | 1.17E-05 | nucleoside phosphate metabolic process |
| GO:0071704 | 1.30E-05 | organic substance metabolic process |
| GO:0003674 | 1.50E-05 | molecular_function |
| GO:0055086 | 1.53E-05 | nucleobase-containing small molecule metabolic process |
| GO:0000166 | 1.65E-05 | nucleotide binding |
| GO:1901265 | 1.65E-05 | nucleoside phosphate binding |
| GO:0007275 | 1.73E-05 | multicellular organism development |
| GO:0048731 | 1.86E-05 | system development |
| GO:0044237 | 2.21E-05 | cellular metabolic process |
| GO:0097159 | 2.62E-05 | organic cyclic compound binding |
| GO:0005488 | 2.66E-05 | binding |
| GO:0044707 | 2.95E-05 | NA |
| GO:0032501 | 2.97E-05 | multicellular organismal process |

| **Table S7.** Immunoblot quantification of STS1-HET and STS1-HOM | | | | |
|---|---|---|---|---|
| **Genotype** | **STS1** | **TUB** | **Relative intensity** | **Relative intensity to HET** |
| *sts1* | 0 | 30242.43 | 0 | 0 |
| *sts1; STS1-HET* | 17705.066 | 23658.492 | 0.74835987 | 1 |
| *sts1* | 0 | 31542.463 | 0 | 0 |
| *sts1; STS1-HOM* | 149610.474 | 25640.48 | 5.834932653 | 7.796960909 |

| **Table S8.** Primers for genotyping assays and RT-qPCR. | | |
|---|---|---|
| **Primer Name** | **Sequence** | **PCR/Genotyping Protocol** |
| STS1 R | GCATCCAGCAGTCTAATTGT | Bpu10I digest<br>Wild type is cut twice<br>sts1is cut once |
| STS1 F | TCGGATAGGGGAACAGACAG | |
| SI1 F | GAGGATCTGGACAGTCTGGACTCC | Wild type: 1 band, heterozygous: three bands, mutant: 2 bands with triplex PCR |
| SI1 R | AGTCTGCGTGCTGATCACATG | |
| MuTIR6 | AGAGAAGCCAACGCCAWCGCCTCYATTTCGTC | |
| YFP F | CGCTGAGCGGCAGCATGAGAGAG | PCR is presence/absence. Or BASTA screen with 1:20 dilution of BASTA |
| YFP R | GTTGGGGTCTTTGCTCAGGGCGG | |
| STS1 (qPCR) F | ATAATGGACTGACGAACCTGAATG | qPCR |
| STS1 (qPCR) R | AGTCTGCGTGCTGATCACATG | |
| SI1 (qPCR) F | CACAGAGATTAGGCAAAGGATGG | qPCR |
| SI1 (qPCR) R | AGTCTGCGTGCTGATCACATG | |
| Actin F | GATTCCTGGGATTGCCGAT | qPCR |
| Actin R | TCTGCTGCTGAAAAGTGCTGAG | |
| STS1-HET/HOM F | TCGGATAGGGGAACAGACAG | Fok1 digest |
| STS1-HET/HOM R | ATCAGGTCTTTGGGTTGCAG | HET variant is not cut, HOM G81D varient cuts once |

**Supplemental Figure Legends**

**Figure S1.** (**A-C**) STS1 immunolocalizations using a polyclonal anti-STS1 antibody in (**A**) STS1-HET, (**B**) STS1-HOM and (**C**) *sts1* mutant flowers. (**D-F**) *in situ* hybridizations of *STS1* mRNA in (**D**) *STS1-HET* and (**E**) *STS1-HOM* (**F**) *sts1* mutant flowers.

**Figure S2.** eFourier analysis of morphospaces occupied by anthers of *sts1* mutants complemented with *STS1-HET* vs *STS1-HOM*

**Figure S3.** STS1-HET is less abundant than STS1-HOM (**A-B**) anti-GFP immunoblot of (**A**) STS1-HET and (**B**) STS1-HOM samples analyzed using mass spectrometry. (**C-D**) iBAQ levels in (**C**) STS1-HET vs *sts1* mutant siblings and (**D**) STS1-HOM vs *sts1* mutant siblings. SI1 levels are similar between STS1-HET and STS1-HOM IPs.

**Figure S4.** GO-term correlation plot comparing probabilities of GO-term enrichments between IP-MS and RNA-Seq datasets. (**B**) STS1-HET IP-MS vs. STS1-HET RNA-Seq.Dot sizes are proportional to the number of genes in each enriched GO-term category. (**B**) STS1-HET IP-MS vs. STS1-HET RNA-Seq. Dot sizes are proportional to the number of genes in each enriched GO-term category, and colored according to which larger category they are associated with. P-value cutoffs for sectors: (i) p-value x > 0.25 & p-value y < 0.01; (ii) 0.01 < p-value x < 0.25 & p.value y < 0.01; (iii) p-value x < 0.01 & p-value y < 0.01; (iv) p.value x < 0.01 & 0.01 < p-value y < 0.25; (v) p-value x < 0.01 & p-value x > 0.25.

**Supplemental Figures**

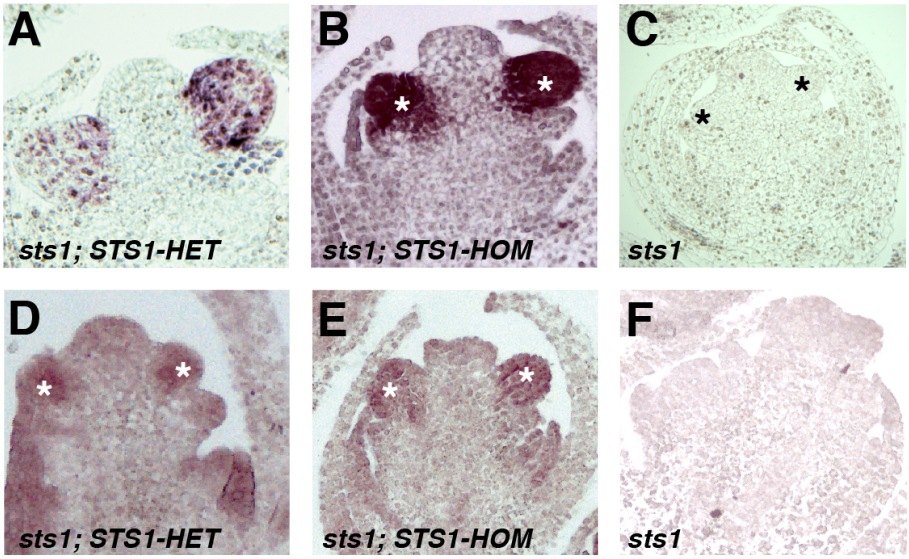


**Figure S1.** (**A-C**) STS1 immunolocalizations using a polyclonal anti-STS1 antibody in (**A**) STS1-HET, (**B**) STS1-HOM and (**C**) *sts1* mutant flowers. (**D-F**) *in situ* hybridizations of *STS1* mRNA in (**D**) *STS1-HET* and (**E**) *STS1-HOM* (**F**) *sts1* mutant flowers.

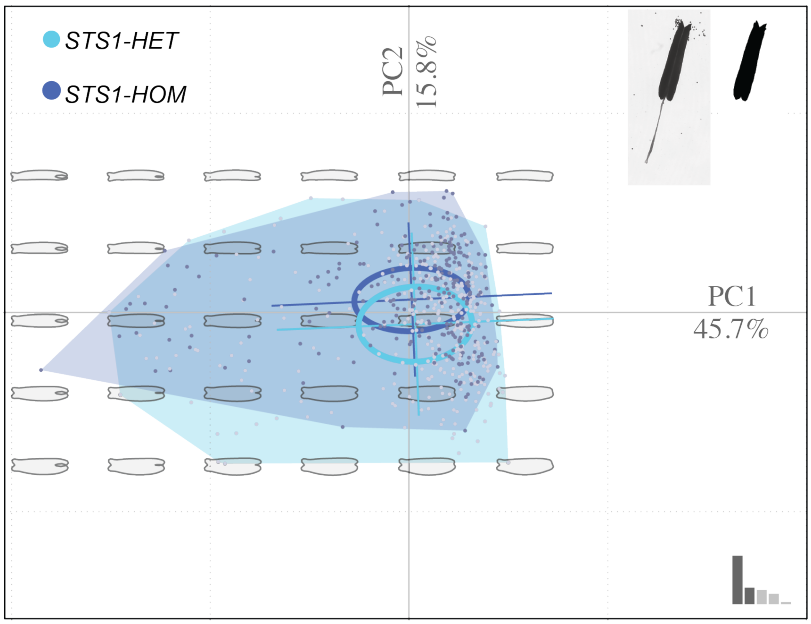


**Figure S2.** eFourier analysis of morphospaces occupied by anthers of *sts1* mutants complemented with *STS1-HET* vs *STS1-HOM*

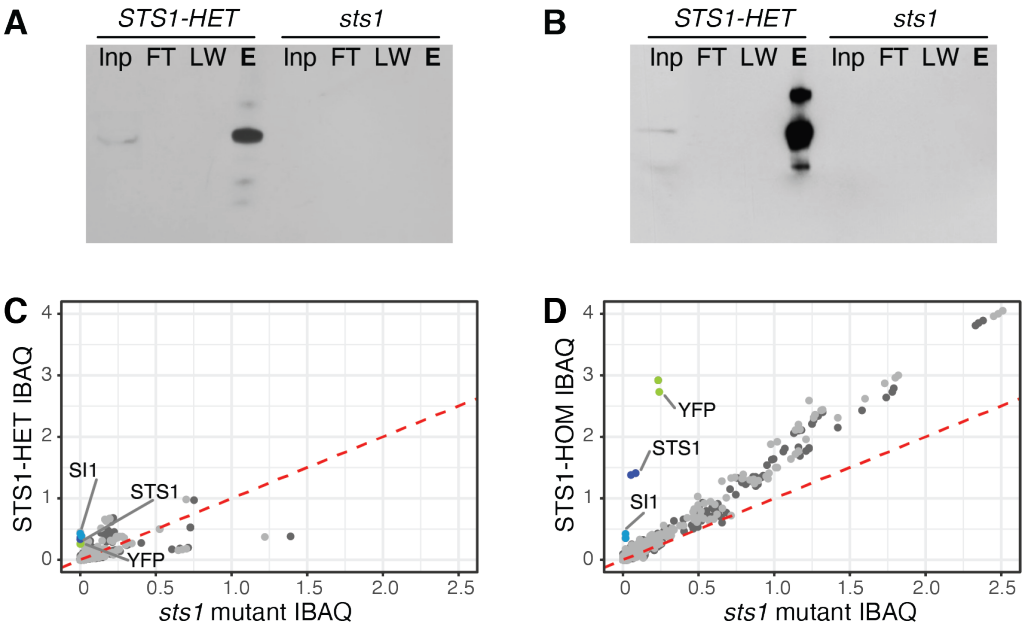


**Figure S3.** STS1-HET is less abundant than STS1-HOM (**A-B**) anti-GFP immunoblot of (**A**) STS1-HET and (**B**) STS1-HOM samples analyzed using mass spectrometry. (**C-D**) iBAQ levels in (**C**) STS1-HET vs *sts1* mutant siblings and (**D**) STS1-HOM vs *sts1* mutant siblings. SI1 levels are similar between STS1-HET and STS1-HOM IPs.

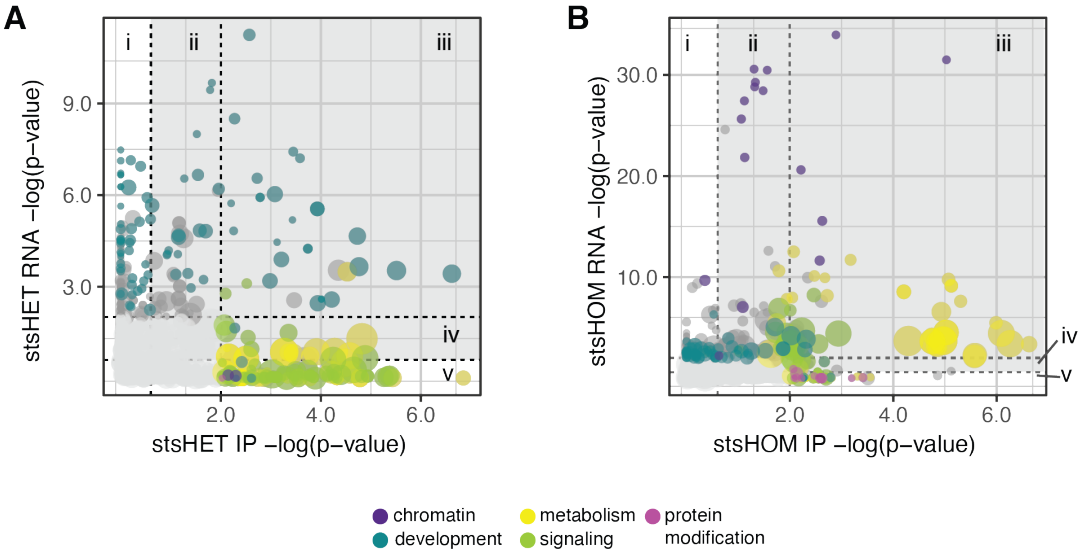


**Figure S4.** GO-term correlation plot comparing probabilities of GO-term enrichments between IP-MS and RNA-Seq datasets. (**B**) STS1-HET IP-MS vs. STS1-HET RNA-Seq.Dot sizes are proportional to the number of genes in each enriched GO-term category. (**B**) STS1-HET IP-MS vs. STS1-HET RNA-Seq. Dot sizes are proportional to the number of genes in each enriched GO-term category, and colored according to which larger category they are associated with. P-value cutoffs for sectors: (i) p-value x > 0.25 & p-value y < 0.01; (ii) 0.01 < p-value x < 0.25 & p.value y < 0.01; (iii) p-value x < 0.01 & p-value y < 0.01; (iv) p.value x < 0.01 & 0.01 < p-value y < 0.25; (v) p-value x < 0.01 & p-value x > 0.25.

**Supplemental References**


1. A. Dobin, *et al.*, STAR: ultrafast universal RNA-seq aligner. *Bioinformatics* 29, 15–21 (2013).
2. Y. Jiao, *et al.*, Improved maize reference genome with single-molecule technologies. *Nature* 546, 524–527 (2017).
3. M. D. Robinson, D. J. McCarthy, G. K. Smyth, edgeR: a Bioconductor package for differential expression analysis of digital gene expression data. *Bioinformatics* 26, 139–140 (2010).
4. D. J. McCarthy, Y. Chen, G. K. Smyth, Differential expression analysis of multifactor RNA-Seq experiments with respect to biological variation. *Nucleic Acids Res.* 40, 4288–4297 (2012).
5. D. Risso, J. Ngai, T. P. Speed, S. Dudoit, Normalization of RNA-seq data using factor analysis of control genes or samples. *Nat. Biotechnol.* 32, 896–902 (2014).
6. C. A. Schneider, W. S. Rasband, K. W. Eliceiri, NIH Image to ImageJ: 25 years of image analysis. *Nat. Methods* 9, 671–675 (2012).
7. V. Bonhomme, S. Picq, C. Gaucherel, J. Claude, Others, Momocs: outline analysis using R. *J. Stat. Softw.* 56, 1–24 (2014).
8. M. Bartlett, *et al.*, Evolutionary Dynamics of Floral Homeotic Transcription Factor Protein–Protein Interactions. *Mol. Biol. Evol.* 33, 1486–1501 (2016).